JOURNAL OF MATERIALS SCIENCE **33** (1998) 4929–4936

Thermodynamic calculation of phase equilibria in the Ti–Co and Ni–Sn systems

P. NASH, H. CHOO
Mechanical, Materials and Aerospace Engineering Dept., Illinois Institute of Technology, Chicago, IL 60616
E-mail: nash@charlie.iit.edu

R. B. SCHWARZ
MST-8, Mail Stop K-765, Los Alamos National Laboratory, Los Alamos, NM 87545
E-mail: rxzs@lanl.gov

A thermodynamic model for the titanium-cobalt system has been developed utilizing measured enthalpies of mixing of the liquid and evaluated phase-diagram data. The free energies of the liquid, bcc, fcc, and hcp solid solutions, and TiCo, Ti_2Co, $TiCo_2$, and $TiCo_3$ compounds were calculated for a temperature of 400 K. The model and measured heats of crystallization have been used to predict the free energy of the metastable amorphous phase at 400 K, needed for comparison with experimental results on the mechanical alloying of Ti and Co. The predicted glass-forming range for alloys prepared by mechanical alloying is from 10 to 81.5 at. % Co. We adopted a similar approach for modeling the Ni–Sn system to calculate the free energies of Ni_3Sn, and Ni_3Sn_2, and the liquid (amorphous) and fcc solid solutions in the nickel-rich region at 240 K. In this system the inclusion of the magnetic contribution to the free energy of the Ni-rich fcc solid solution is important in interpreting the results of mechanical alloying. We propose a simple transformation of the free-energy curves, which assists in the graphical identification of the glass-forming ranges.

1. Introduction

Thermodynamic models of alloy systems are needed for interpreting and predicting metastable-phase formation brought about by novel processing techniques such as rapid solidification and mechanical alloying. Unfortunately, it is rare that sufficient thermodynamic data exists to accurately formulate such models. More often the models must be developed using limited thermodynamic data and evaluated phase-diagram data. Although thermodynamic models are based mainly on high-temperature data, assuming that the model reasonably represents the known data [1], it is possible to extrapolate the free-energy functions to lower temperature since they vary smoothly with temperature. A previous thermodynamic model of the Ti–Co system does not provide consistent phase relationships at low temperatures [2] and cannot be used for the present purpose of extrapolation to low temperatures. The CALPHAD approach [3] has been used in this work to develop thermodynamic models of Ti–Co and Ni–Sn and to assist in the interpretation of the results obtained from mechanically alloying a range of compositions from these systems.

2. Thermodynamic models

The free energy of a solution phase in a binary metallic system is described by an expression of the form,

$$G^i = G^i_1 x_1 + G^i_2 x_2 + RT(x_1 \ln x_1 + x_2 \ln x_2) + G^i_{ex} \quad (1)$$

where G^i_1 and G^i_2 are the lattice stabilities (i.e., reference chemical potentials) of the pure components. $x_1 (= 1 - x_2)$ is the molar fraction of component 1. G^i_{ex} is the excess free energy of mixing of the phase i. G^i_{ex} can be described by a polynomial, in this case a Legendre polynomial of the form

$$G^i_{ex} = x_1 x_2 \{A^i + B^i T + (C^i + D^i T)(1 - 2x_1) + (E^i + F^i T)(6x_1^2 - 6x_1 + 1)\} \quad (2)$$

where A^i, B^i, C^i, D^i, E^i and F^i are the polynomial coefficients or interaction parameters.

G^i for the intermetallic phases may also be expressed by a solution model, or by a sublattice model, but if the compounds exist over a narrow homogeneity range, they are generally assumed to be line compounds and the G^i require no composition terms. Thus, for the compounds we use

$$G^i = H^i - TS^i \quad (3)$$

2.1. Thermodynamic model for the Ti–Co system

The lattice stability parameters for Ti and Co [3], listed in Table I, were used as a starting point for the modeling procedure. Slight modifications were made in some cases due to revised heats of transition and

0022–2461

TABLE I Lattice stability parameters of cobalt, titanium, nickel, and tin (units of J mole^{-1} and J mole^{-1} K^{-1}), referred to the liquid standard state

$G^{hcp_{Co}} = -17591 + 10.334T$
$G^{hcp_{Ti}} = -21725 + 13.38T$
$G^{bcc_{Co}} = -11339 + 6.568T$
$G^{bcc_{Ti}} = -15450 + 7.95T$
$G^{fcc_{Co}} = -17155 + 9.706T$
$G^{fcc_{Ti}} = -17238 + 12.134T$
$G^{fcc_{Ni}} = -17486 + 10.12T$
$G^{fcc_{Sn}} = -418.5 + 6.67T$

TABLE II Calculated interaction parameters for the solution phases in the Ti–Co system. For these phases the interaction parameters D, E, and F are all zero

Phase	A (J mole^{-1})	B (J mole^{-1} K^{-1})	C (J mole^{-1})
Hexagonal	−80,000	32	−12,000
BCC	−105,000	30	−20,000
FCC	−125,000	48.3	−14,000
Liquid	−145,840	40	−19,933

TABLE III Calculated Gibbs free energy for the compounds in the Ti–Co system (units of J mole^{-1} and J mole^{-1} K^{-1})

$G^{TiCo} = -59825 + 17.980T$
$G^{Ti_2Co} = -72000 + 32.140T$
$G^{TiCo_2} = -49952 + 16.35T$
$G^{TiCo_3} = -42800 + 14.6T$

melting points [4]. Esin et al. [5] measured the enthalpies of mixing of liquid $Ti_{1-x}Co_x$ for $x = 0.45$ to 1.0 at 2000 K. Their result can be described by the polynomial:

$$\Delta H_{mix}^{Ti-Co} = x(1-x)[-145,840 + 19,933(1-2x)](J\,mole^{-1}) \quad (4)$$

Since there is no data on the temperature dependence of the heat of mixing, we allowed the temperature-dependent interaction parameter to be a variable in the optimization procedure described later. No experimental data have been reported on partial Gibbs free energies or heats of formation of the compounds. Invariant temperatures and compositions of the phases involved can be used to help determine consistent thermodynamic parameters, since the necessary condition is that the respective free-energy curves have a common tangent at the specific equilibrium-phase compositions. Invariant phase compositions and temperatures were obtained for all of the reactions occurring in this system from the evaluated-phase diagram [2], Fig. 1a.

Equilibrium in two phase regions also requires common tangents between the free energy curves of the phases at their respective compositions. Such data down to 873 K were obtained from the evaluated-phase diagram. Similarly, congruent melting temperatures provide information on the equality of the free energies of the solid and liquid phases. Using the interaction parameters *A* and *C* for the liquid phase and the evaluated equilibrium phase diagram data discussed above, we derived complete temperature-dependent interaction parameters for the phases (liquid, hcp, bcc, fcc, TiCo, Ti_2Co, $TiCo_2$, and $TiCo_3$). Initial values for the parameters were obtained from a least-squares optimization procedure provided in the computational thermodynamics program [6]. Final values for the parameters were obtained by a trial and error procedure aimed at improving the fit between the calculated and experimental phase diagrams. The interaction parameters obtained are listed in Tables II and III. The phase diagram calculated from these parameters is shown in Fig. 1b. The *α–Co* solvus (dashed line) was only estimated down to 1173 K, since below this temperature it is affected by the magnetic-ordering energy. This contribution was not evaluated for the TiCo system, since it affects both the fcc and hcp phases and will only provide a small change in free energy. Using the interaction parameters derived from the optimization, we calculated the free energy curves for the liquid, bcc, fcc, and hcp phases of the Ti–Co system at the temperature of 400 K (Fig. 2). This temperature is believed to approximate the reaction temperature during mechanical alloying in an air-cooled SPEX mill [7]. This diagram also shows the calculated free energies of Ti_2Co, TiCo, $TiCo_2$, and $TiCo_3$.

In Fig. 2, the free energy of the undercooled liquid (extrapolated to 400 K) overestimates the free energy of the amorphous or glassy phase. This is because as the temperature decreases below the melting temperature and approaches the glass-transition temperature, T_g, the specific heat of the undercooled liquid first increases, reaching a peak near $T_g + 50$ K, and then decreases to a value close to that of the crystalline phase(s). This peak is associated with the rapid decrease in the liquid's configurational degrees of freedom as its temperature approaches T_g and becomes a glass. Because the thermodynamic modeling is based on equilibrium data, it cannot take into account the change in c_p of the undercooled (metastable) liquid phase. Thus, the liquid-free energy curve, extrapolated to 400 K, represents an upper limit to the free energy of the amorphous phase. Several models have been developed [8] that give estimates for the free energy of elemental amorphous phases, but these are not directly applicable to binary alloy systems. If we assume that the excess specific heat associated with the glass transition is independent of composition, then the free-energy curve of the amorphous phase could be obtained by shifting down the free-energy curve of the undercooled liquid. The amount of the free-energy shift can be inferred from the excess specific-heat models for the pure elements. The amorphous free-energy curve obtained in this way assumes that the amorphous phase has no short-range order (SRO). Recent elastic constant measurements [9] show, however, that amorphous Ni–Zr alloys prepared by the condensation of metallic vapors exhibit SRO, which is accentuated near the compositions at which Ni and Zr form equilibrium crystalline intermetallics. In order to take into account the increased stability of the amorphous phase due to SRO, it is preferable to determine the free energy shift from measured enthalpies

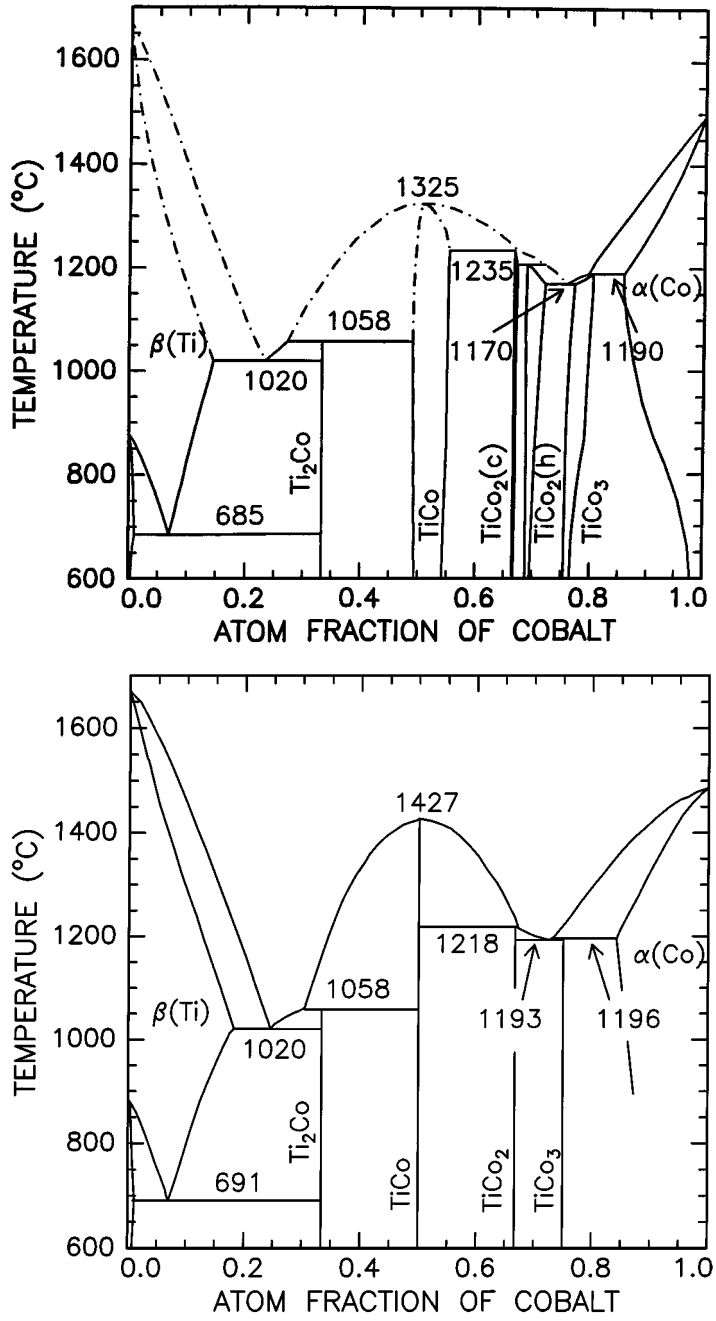

Figure 1 (a) Evaluated phase diagram for the Ti–Co system from [2] (b) Calculated Phase diagram for the Ti–Co system.

of crystallization of alloys. We have taken here the latter approach, using the enthalpy of crystallization of $Ti_{0.25}Co_{0.75}$, measured by Vuorinen and Tiainen [10]. To obtain the free energy of the amorphous phase, we shifted down the free energy of the liquid phase, so that the difference between the free energies of amorphous and crystalline $Ti_{0.25}Co_{0.75}$ equals the measured value, 2.98 kJ mole^{-1}. This required shifting the free energy of the undercooled liquid by -10 kJ mole^{-1}.

The free-energy diagram in Fig. 2 can be used to predict the glass-forming range (GFR) for amorphous alloys prepared by isothermal methods (solid state reactions and mechanical alloying). However, the closeness of the free-energy curves and the similarity in their slopes makes the graphical identification of the tangency points rather difficult. Fig. 3 shows the same free-energy curves after subtracting from each one the free energy of the liquid phase. Thus, in Fig. 3, the free energy of the undercooled liquid is simply $y = 0$ kJ mole^{-1} and the free energy of the amorphous phase is $y = -10$ kJ mole^{-1}. A clear advantage of this transformed diagram is that the intersections of the various free-energy curves are easier to locate visually than in Fig. 2. The two solid curves are the common tangents calculated from the data in Fig. 2 and then transformed: the left one between the amorphous and hexagonal β-Ti(Co) solid solution phases, and the right one between the amorphous and the fcc α-Co(Ti) solid-solution phases. Notice that the transformed common tangents osculate the free-energy curves, as required. The small ticks identify the osculation points.

Fig. 3 can now be used to predict glass-forming ranges expected when preparing amorphous alloys by solid state reactions or by mechanical alloying. For solid-state reactions at 400 K, the expected GFR is determined by the common tangents (now transformed

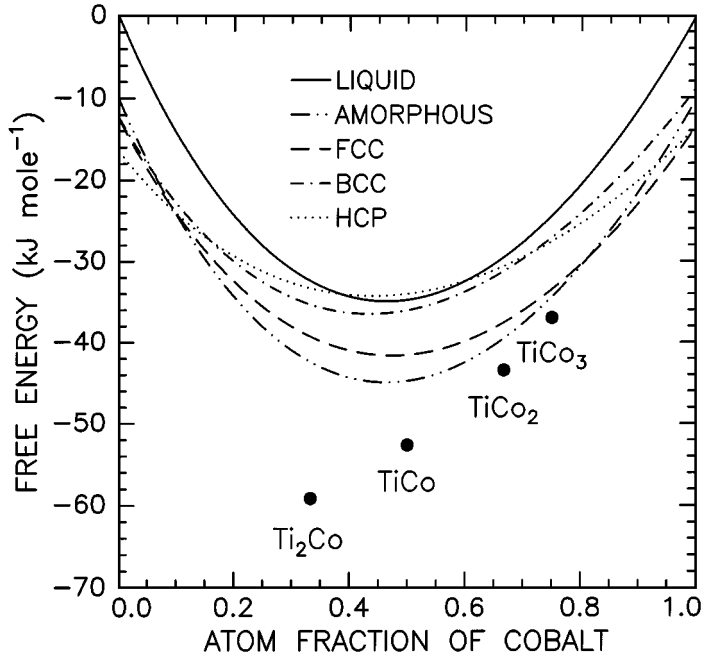

Figure 2 Calculated free-energy relationships for the Ti–Co system at 400 K.

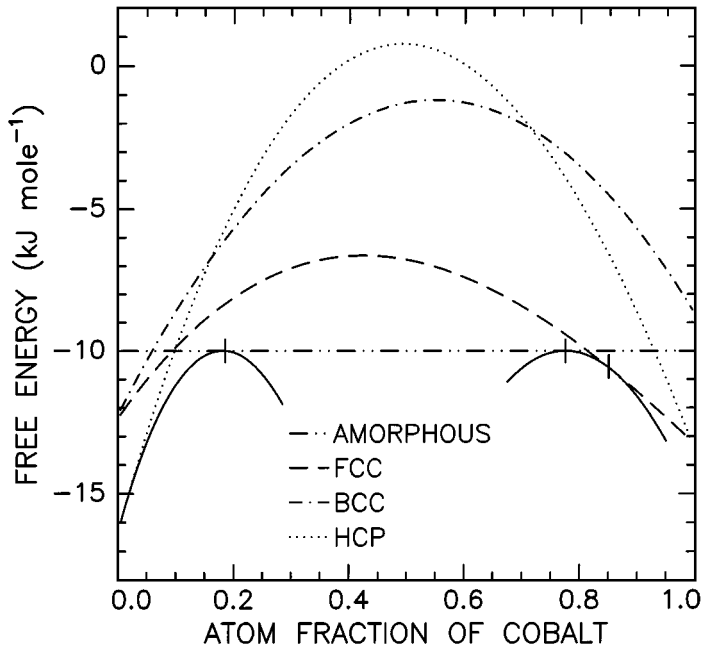

Figure 3 Calculated free-energy relationships for the Ti–Co system at 400 K, plotted in a transformed coordinate system in which the free energy of the amorphous phase is $y = 0$.

into curves) and thus extends from 0.185 to 0.775 atom fraction cobalt. For $0.005 < x < 0.185$, the amorphous phase would coexist with hcp Ti(Co), whereas for $0.775 < x < 0.85$, the amorphous phase would coexist with fcc Co(Ti). For mechanical alloying at 400 K, the GFR is determined by the extent to which the free-energy curve (now line) for the amorphous phase is lower than that of any of the crystalline solid solutions. This is because in the mechanical alloying process, where the particles are successively fractured and cold welded, the amorphous product cannot partition to lower its free energy [11]. Thus the GFR expected for powder prepared by mechanically alloying titanium and cobalt powder should extend from about 0.1 to 0.815. Outside this range, the product should be hcp Ti(Co) and fcc Co(Ti), respectively. For $x \approx 1.0$, the product should be hcp Co(Ti). Amorphous compositions of $Ti_{50}Co_{50}$, $Ti_{40}Co_{60}$ and $Ti_{25}Co_{75}$ have been prepared by mechanical alloying [10, 12–14]. The glass-forming range for alloys prepared by magnetron sputtering has been determined to extend from 23 to 73 at. % cobalt [15]. $Ti_{77}Co_{23}$ and $Ti_{22}Co_{78}$ alloys prepared by melt spinning were also found to be amorphous [16]. Thus the glass-forming range predicted from our thermodynamic model encompasses all of the amorphous compositions found experimentally. Several metastable alloys in the Ti–Co system were produced by mechanically alloying elemental powder blends [13]. The free

energy of an elemental mixture of powders at the average composition $Ti_{52}Co_{48}$ is given by

$$G_{mix} = 0.52G_{Ti}^{hcp} + 0.48G_{Co}^{hcp} \quad (5)$$

and from examination of Fig. 2 it is clear that any of the alloy phases may be formed, since that would result in a decrease in free energy. The x-ray diffraction results show that after milling the $Ti_{52}Co_{48}$ blend for a short time, the TiCo intermetallic compound forms first, followed, after longer milling times, by amorphization. A similar result has been observed by Koch and Kim for Nb_3Sn and Nb_3Ge [17]. An interesting feature of the Ti–Co system is that the compound TiCo has the B2–CsCl structure and can be considered as an ordered form of a $Ti_{50}Co_{50}$ bcc solid solution. Thus the ordering energy is directly obtainable from the free-energy diagram in Fig. 2 as –16.6 kJ mole^{-1}. If antisite defects are gradually introduced into ordered TiCo, its free energy could be raised until it has become a disordered bcc solid solution. Because the disordered bcc phase is not observed for long mechanical alloying times (amorphization occurs first), one must conclude that the free energy curve of the amorphous phase at $x = 0.50$ lies below that for the bcc solid-solution phase. This agrees with our calculation, which shows (Figs. 2 and 3) the -10 kJ mole^{-1} shift of the undercooled liquid free energy curve produces an amorphous free energy lower than the free energy of the bcc phase at this composition. As anti-site defects are introduced through mechanical alloying, the free energy of the partially disordered compound exceeds that of the amorphous phase, and it becomes energetically favorable for this structure to transform to the amorphous phase. Thus the increase in free energy required to amorphize fully ordered TiCo, $\Delta G_{\text{TiCo-amorphous}} = 7.9$ kJ mole^{-1} can be fully accommodated through the introduction of anti-site defects.

2.2. Thermodynamic model for the Ni–Sn system

The evaluated Ni–Sn phase diagram from [18] is shown in Fig. 4 with solid lines and our calculated Ni–Sn diagram with dashed lines. The thermodynamic model was developed using available thermodynamic and phase-equilibrium data as described above for the Ti–Co system. The lattice-stability terms for fcc nickel and tin were taken from [3] with slight modifications for revised heats of transition [4]. Eremenko et al. [19] determined integral free energies, G^L, for liquid $Ni_{1-x}Sn_x$ alloys at 1573 K. From this data we determined the excess free energy, G_{ex}^L and fitted this data to a cubic polynomial to obtain the following composition dependence:

$$G_{ex}^L = -85.3415x^3 + 188.765x^2 - 103.454x, \quad (6)$$

where x is the mole fraction of Sn. Note that the coefficients obtained are slightly different than those given in [20]. Using Equation 6 we derived the interaction parameters for the liquid phase given in Table IV. Fig. 5 compares the calculated liquid free energies of formation with the experimental data, and the agreement is seen to be reasonable.

The thermodynamic parameters for Ni_3Sn_2 and for the high-temperature (HT) form of Ni_3Sn (HT) were derived using Equation 3, the enthalpy of formation

TABLE IV Calculated interaction parameters for the solution phases in the Ni–Sn system. For these phases the interaction parameters B, D, and F are all zero

Phase	A (J mole^{-1})	C (J mole^{-1})	E (J mole^{-1})
FCC	−45,000	−12,000	−39,500
Liquid	−60,340	−24,330	0

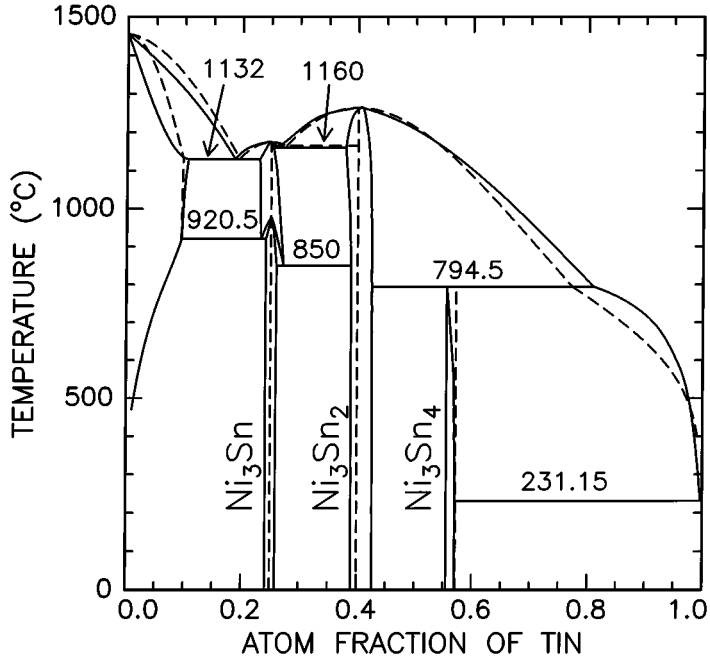

Figure 4 Ni–Sn phase diagrams. Full line: evaluated diagram from [18]; dashed line: calculated diagram (present work).

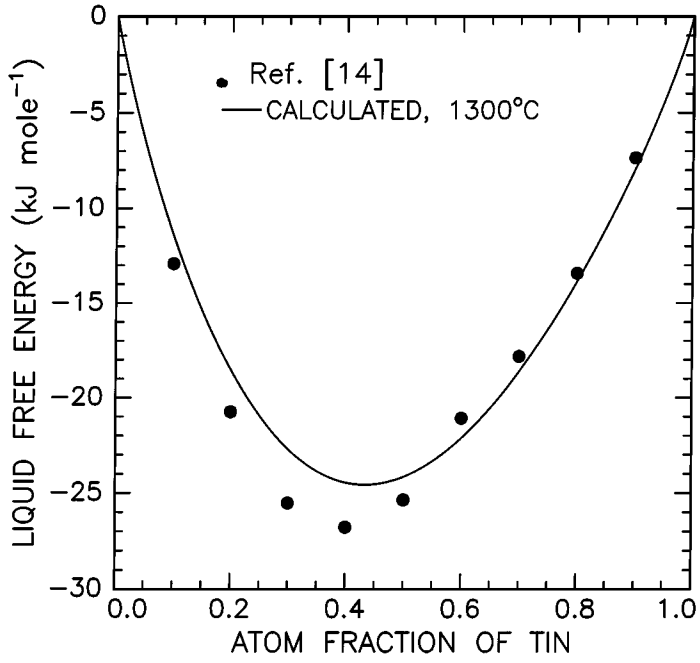

Figure 5 Calculated and measured free energy of mixing in liquid Ni–Sn alloys at 1300 °C.

data of references [21, 22], and setting their free energies equal to that of the liquid at their respective congruent melting points. The compound parameters for the low-temperature (LT) form Ni_3Sn (LT) were found using Equation 3 and setting its free energy equal to that of Ni_3Sn(HT) at 920.5 °C. Since the model simplifies the system by assuming all intermediate phases are line compounds (Fig. 4), the two eutectoid reactions involving Ni_3Sn(LT) and Ni_3Sn(HT) at T = 920.5 °C and T = 850 °C, respectively, cannot both be reproduced. The reaction Ni_3Sn (HT) $\leftrightarrow$ (Ni) + Ni_3Sn (LT) at 920.5 °C was selected as the one at which the free energies of the two phases are equal. For the purposes of this work, this simplification does not affect the conclusions drawn on the basis of the thermodynamic model. Table V gives the free energy of formation of the Ni–Sn compounds.

The thermodynamic parameters of the nickel solid solution were derived by adjusting them to reproduce the eutectic (1132 °C) and eutectoid (920.5 °C) transformations, both in terms of temperature and composition and keeping the liquid and Ni_3Sn (LT and HT) parameters constant. The parameters of the Ni_3Sn compound were derived by fixing the peritectic temperature equal to the experimental value (794.5 °C) and attempting to reproduce the Ni_3Sn_4 liquidus. The equilibrium tin terminal solid solution was not modeled in this work.

Fig. 6 shows the free-energy of the nickel-rich end of the Ni–Sn system evaluated at 240 K. The solid curve is the calculated free energy of the undercooled liquid. As we discussed previously, this extrapolated curve overestimates the free energy of the amorphous phase. To derive the free energy of the amorphous alloy phase, we assumed that the *composition* dependencies of the undercooled liquid and amorphous phases are the same. We then constructed the amorphous curve by shifting the liquid curve downwards in parallel fashion. The downward shift is such that at the composition $Ni_{75}Sn_{25}$, the difference between the free energies of the amorphous and crystalline Ni_3Sn phases at 240 K equals the measured crystallization enthalpy [23]. The dashed curve is the free energy of the crystalline Ni-rich terminal solid solution derived from the thermodynamic model. At low temperatures the magnetic contribution to the free energy of the Nickel solid solution phase needs to be considered. The magnetic contribution to the free energy of the (Ni) fcc phase was determined from [24].

$$\Delta G_m = -0.9RT_c\{\ln(\beta^0 + 1)\}(\beta^T/\beta^0) - RT\ln((\beta^0 - \beta^T) + 1) \quad (7)$$

where T_c is the Curie temperature at a given composition, which was obtained from [18], and β^T and β^0 are the average magnetic moments per atom in Bohr magnetons at a given composition for temperature T and T = 0 K respectively.

The dotted curve corresponds to the magnetic fcc Ni(Sn) solid solution. Also added to the figure are the free energies of the Ni_3Sn and Ni_3Sn_2 crystalline intermetallic compounds (open circles) derived from the model.

Ball milling of $Ni_{1-x}Sn_x$ alloys was performed at 240 K by cooling the milling vial with a stream of liquid nitrogen. The various phases formed by mechanical alloying were reported in [23]. It was observed

TABLE V Calculated Gibbs Free Energy for the Compounds in the Ni–Sn System (units of J mole^{-1} and J mole^{-1} K^{-1})

$G^{Ni_3Sn(HT)} = -27495 + 4.931T$
$G^{Ni_3Sn(LT)} = -30638 + 7.561T$
$G^{Ni_3Sn_2} = -36989 + 8.2887T$
$G^{Ni_3Sn_4} = -34263 + 12.2T$

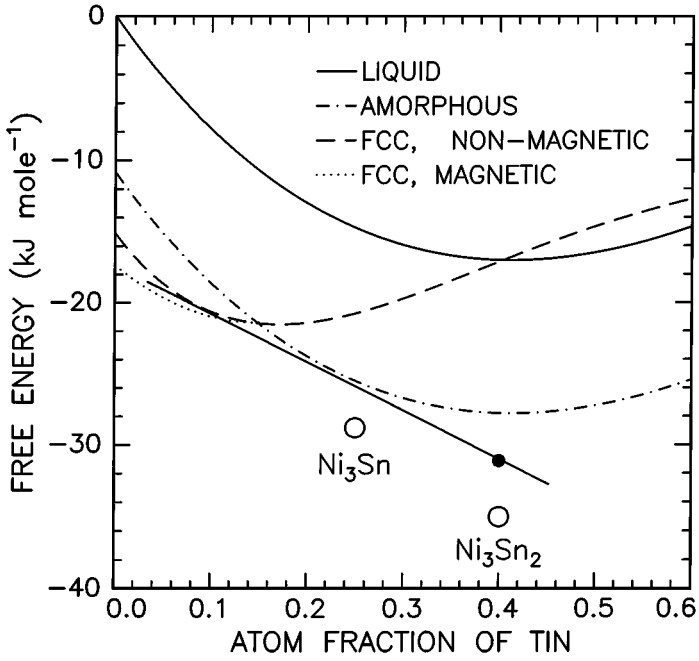

Figure 6 Calculated free energy relationships in Ni–Sn at 240 K.

that for $0.20 < x < 0.25$, the mechanically alloyed product was a two-phase mixture of non-magnetic fcc Ni(Sn) solid solution and amorphous $Ni_{0.75}Sn_{0.25}$. For $0.25 < x < 0.40$, the product was a mixture of amorphous $Ni_{0.75}Sn_{0.25}$ and nanocrystalline Ni_3Sn_2. At $x = 0.40$, the mechanically alloyed product was single-phase nanocrystalline Ni_3Sn_2. The measured enthalpy of transformation from nanocrystalline to crystalline Ni_3Sn_2 was 3.89 kJ mole^{-1}. Using this value and the modeled free energy of large grain crystalline Ni_3Sn_2, we determined the free energy of nanocrystalline Ni_3Sn_2, shown as the solid circle in Fig. 6. Notice that the free energies of nanocrystalline Ni_3Sn_2, the amorphous phase at $x = 0.25$, and the FCC Ni(Sn) solid solution at $x = 0.1$ all lie approximately on the same common tangent (solid line). This explains why amorphous Ni–Sn was only synthesized by mechanical alloying at the composition $x = 0.25$ [23].

Conclusions

Thermodynamic modeling of binary-phase diagrams combined with measured heats of crystallization can be used to obtain the free energy of the amorphous phase. The procedure involves shifting downwards the calculated free-energy curve for the undercooled liquid. The magnitude of the shift may be derived from measured enthalpies of crystallization at the compositions of intermetallics. This procedure should be more accurate than basing the shift on estimated values of $G_{liq} - G_{am}$ for the pure elements.

A simple transformation of the free-energy curves obtained by subtracting the free energy of the undercooled liquid results in a diagram, which enables a clearer visualization of the glass-forming ranges for amorphous alloys synthesized by isothermal transformations and reactions. The glass-forming range predicted from the thermodynamic model in the Ti–Co system for alloys synthesized by MA extends from 10 to 81.5 at. % cobalt. The glass-forming range predicted by the model for the Ni–Sn system corresponds to a single composition at 25 at. % tin, in agreement with the experiment.

Acknowledgements

Part of this work is based on material submitted by H. Choo in partial fulfillment of the M.S. degree at IIT. This work was supported by the U.S. Department of Energy, Office of Basic Energy Sciences, Division of Materials Science. We thank Prof. H. Lukas for providing us a copy of his software.

References

1. R. B. SCHWARZ, P. NASH and D. TURNBULL, J. Mater. Res. **2** (1987) 456–60.
2. J. MURRAY, in "Phase Diagrams of Binary Titanium Alloys," edited by J. Murray, (Amer. Soc. for Metals Int., Metals Park, Ohio, 1987), p. 59.
3. L. KAUFMAN and H. BERNSTEIN, in "Computer Calculation of Phase Diagrams" (Academic Press, New York, 1970).
4. M. W. CHASE, *Bull. Alloy Phase Diagrams* **4** (1983) 123.
5. Y. O. ESIN, M. G. VALISHEV, P. B. GEL'D and M. S. PETRUSHEVSKII, *Zh. Fis. Khim.* **54** (1980) 2267–2270.
6. H. LUKAS, private communication, Max-Planck Institut fur Metallorschung, Stuttgart, 1984.
7. R. B. SCHWARZ and C. C. KOCH, *Appl. Phys. Lett.* **49** (1986) 146.
8. J. H. PEREPEZKO and J. S. PAIK, *J. Non-Cryst. Solids* **61&62** (1984) 113.
9. J. RUBIN and R. B. SCHWARZ, *Phys Rev. B* **50** (1984) 795–804.
10. J. VUORINEN and T. TIAINEN, Tampere University of Technology (unpublished results, 1994).
11. E. MA and M. ATZMON, *Mater. Chem. and Phys.* **39** (1995) 249–267.
12. B. P. DOLGIN, M. A. VANEK, T. MCGORY and D. J. HAM, *J. Non-Crystalline Solids*, **87** (1986) 281–289.
13. H. CHOO, M.S.Thesis (Illinois Institute of Technology, Chicago, 1991).

14. E. HELLSTERN and L. SCHULTZ, *Mater. Sci. And Engineering* **93** (1987) 213–216.
15. R. E. SOMEKH, Z. H. BARBER, C. S. BAXTER, P. E. DONOVAN, J. E. EVETTS and W. M. STOBBS, *J. Mater. Sci. Lett.* **3** (1984) 217.
16. K. H. J. BUSCHOW, *Solid State Communications* **43** (1982) 171–174.
17. C. C. KOCH and M. S. KIM, *J. de Physique, Colloque* **C8** (1985) 573.
18. P. NASH and A. NASH, in "Phase Diagrams of Binary Nickel Alloys" edited by P. Nash (ASM International, Metals Park, Ohio, 1991), pp. 310–318.
19. V. N. EREMENKO, G. M. LUKASHENKO and V. L. PRITULA, *Zh. Fiz. Khim.* **45** (1971) 1993–1995.
20. V. N. EREMENKO, G. M. LUKASHENKO and V. L. PRITULA, *Proc. 4th ICVM*, Sec. 1, 44–46 (1973).
21. F. KORBER and W. OELSON, *Mitt. Kaiser Willhelm Inst. F. Eisenforsch.*, **19** (1937) 209–219.
22. B. PREDEL and W. VOGELBEIN, *Thermochim. Acta* **30**, (1979) 201–215.
23. T. J. TIANEN and R. B. SCHWARZ, *J. of Less-Common Met.* **140** (1988) 99.
24. A. P. MIODOWNIK, *Calphad* **1**(2) (1977) 133.

Received 1 January
and accepted 7 February 1998